6.78 MHz Wireless Power Transmitter Based on a Reconfigurable Class–E Power Amplifier for Multiple Device Charging

Hansik Oh, Wooseok Lee, *Student Member, IEEE*, Hyungmo Koo, Jongseok Bae, *Student Member, IEEE*, Keum Cheol Hwang, *Senior Member, IEEE*, Kang-Yoon Lee, *Senior Member, IEEE*, and Youngoo Yang, *Senior Member, IEEE*

***Abstract*—This article presents a 6.78 MHz wireless power transmitter based on a reconfigurable Class-E power amplifier for various and multiple device charging. To maintain high–efficiency for various power receiving devices, an optimized offset transmission line based on lumped components and a susceptance switching circuit are proposed at the load network of the differential Class-E power amplifier. The offset transmission line changes the load impedances of the Class-E power amplifier for the various receivers to the high-power and high–efficiency region. In addition, the susceptance switching circuit further shifts the load impedances of the Class-E power amplifier for some receivers to the high-power and high–efficiency region. To verify the proposed offset line and susceptance switching circuit, a 6.78 MHz wireless power transmitter was implemented and verified for various receivers. For three different receivers, the transmitter maintains optimal transmission efficiencies for received power levels of 39.7, 16.3, and 8.5 W. A peak system efficiency of 81.4% was achieved when the received power is 31.9 W. The system efficiency maintained well around 74.2 and 70.6% for the received power of 16.3 and 8.5 W, respectively.**

***Index Terms*—Multiple device charging, offset transmission line, reconfigurable Class–E power amplifier, susceptance switching circuit, wireless power transfer.**

I. Introduction

WIRELESS power transfer (WPT) technologies for mobile or wearable devices have been more and more popular, thanks to high user convenience. Inductive coupling, which uses a very low frequency of less than 1 MHz, has been actively applied for various mobile phones and wearable devices. In addition, WPT systems using electromagnetic resonance, which uses little of the higher–frequency bands of 6.78 or 13.56 MHz, has been emerging as an alternative technology [1]–[18].

Research on various circuits for WPT systems based on electromagnetic resonance, which uses the 6.78 MHz band, has been actively done [10]–[17]. In [10], optimal design parameters for the Class-E power amplifier (PA) and the rectifier were calculated for the wide range of the load impedance. It was experimentally verified that the WPT system can be optimized using the calculated values for the various load impedances. An impedance transformation network, which transforms a wide range of the load impedance into the high–efficiency region, was introduced for the Class-E PA [11]. A closed-loop WPT system, which controls the output current of the Class-D PA to optimize the load impedance of the resonator, was proposed for charging mobile devices in [12]. Through the real–time control based on the bluetooth link between the Tx and Rx, it was demonstrated that the maximum system efficiency can be maintained. For [10]–[12], only a single Rx was considered.

WPT systems for multiple Rx's using a single Tx have been also introduced [13]–[14]. Maximum efficiency point can be adaptively tracked by controlling the duty cycle for the buck converter in the Rx [13]. In addition, it was demonstrated that three Rx's can be efficiently charged one by one using time-division multiplexing scheme. Six lithium-ion batteries can be charged and their voltages can be equalized using a single Tx [14]. However, in [13] and [14], multiple but homogeneous Rx's were considered. Resonator design and tuning methods for homogeneous multiple Rx coils were reported in [19]–[21]. In [19], an equivalent circuit model was proposed for a single Tx and multiple Rx's. Optimum distance and resonant capacitor were derived for a frequency of 6.5 MHz. In [20], a switchable matching network using a capacitor array in the resonator was proposed for efficient power transfer. In [21], the power division ratio to the multiple Rx's was derived in terms of the load impedance, inductance, and coupling coefficient. An impedance inverter was proposed to appropriately distribute power to the multiple Rx's. What is needed is a Tx that can charge multiple and different Rx's and maintain high-efficiency for various charging conditions.

In this article, a 6.78 MHz Tx for a WPT system that can charge multiple and different Rx's with high-efficiency is proposed. An offset transmission line (OTL) at the load network of the Class-E PA is proposed to maintain high-efficiency for the various load impedances from the various configurations of multiple Rx's. In addition, a simple susceptance switching

Manuscript received April 9, 2019; revised July 18, 2019 and September 24, 2019; accepted November 11, 2019. Date of publication November 14, 2019; date of current version February 20, 2020. This work was supported by the National Research Foundation of Korea (NRF) grant funded by the Korean government (MSIP) under Grant 2014R1A5A1011478. Recommended for publication by Associate Editor Prof. Michael (GE) A. E. Andersen. *(Corresponding author: Youngoo Yang.)*

The authors are with the Department of Electrical and Computer Engineering, Sungkyunkwan University, Suwon, 16419, Korea (e-mail: 5hansike@gmail.com; ws02.lee@gmail.com; 99hyungmo@gmail.com; baeyas0@gmail.com; khwang@skku.edu; klee@skku.edu; yang09@skku.edu).

Digital Object Identifier 10.1109/TPEL.2019.2953719

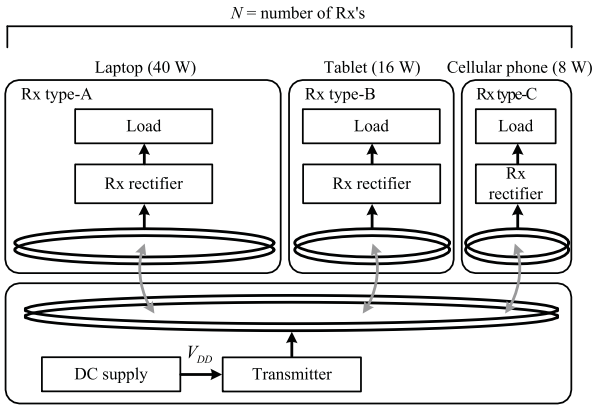

Fig. 1. WPT system for multiple charging using three different types of Rx's.

circuit (SSC) is proposed to the load network of the Class-E PA that can further tune the load impedance which is changed too much for some cases. The OTL works without control, while the SSC requires just a two-bit digital control for various Rx conditions. It was experimentally demonstrated, for the first time, that the Class-E Tx using the proposed OTL and the SSC maintains high-efficiency for various homogeneous or heterogeneous configurations of multiple Rx's.

Design procedure for the optimized OTL and the SSC will be presented according to the load impedances of the Class–E PA for the nine charging cases using the three types of Rx's. Comparative experimental results for the conventional configuration without the OTL and the SSC, the second configuration with the OTL and without the SSC, and the third configuration with the OTL and the SSC will be presented. The experimental results will be compared to the previously reported state-of-the-art as well.

II. Multiple Charging Scenarios and TX Load Impedances

A. Various Cases for Single or Multiple Charging

A configuration of the WPT system, which can charge various types of mobile devices, such as laptops, tablets, or cellular phones, is shown in Fig. 1. For three possible types of mobile devices, Rx circuits should be differently designed. Laptops can have Rx type-A which is designed to output a dc power of about 40 W. Tablets can have Rx type-B which is designed to output a dc power of about 16 W. Cellular phones can have Rx type-C which is designed to output a dc power of about 8 W. Each Rx type has different resonant coils whose sizes were determined to fit the sizes of the application devices.

Nine different cases using various combinations of the three types (A, B, and C) of Rx's are selected for representative single or multiple Rx configuration, as shown in Table I. Case 1, 3, and 9 are configured with a single Rx using type-A, -B, and -C, respectively. Case 4 and 5 are configured with heterogeneous multiple Rx's using one type-B and two type-C Rx's and using one type-B and one type-C Rx's, respectively. Case 2, 6, 7, and 8 are configured with homogeneous multiple Rx's using two type-B, four type-C, three type-C, and two type-C Rx's, respectively.

TABLE I
Selected Cases for Various Single or Multiple Rx's

Case	Rx type (number of Rx's)	Charging type
1	A (1)	Single
2	B (2)	Homogeneous multiple
3	B (1)	Single
4	B (1), C (2)	Heterogeneous multiple
5	B (1), C (1)	Heterogeneous multiple
6	C (4)	Homogeneous multiple
7	C (3)	Homogeneous multiple
8	C (2)	Homogeneous multiple
9	C (1)	Single

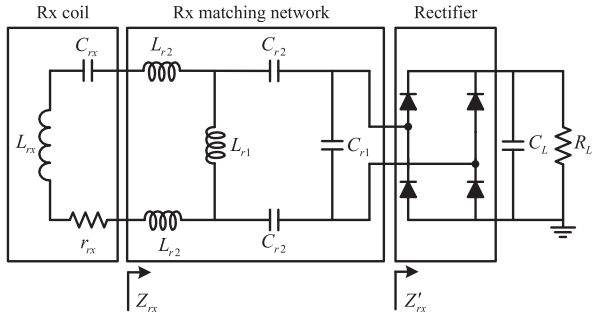

Fig. 2. Schematic of the Rx using a full-bridge rectifier.

B. Rx Circuit and Resonant Coil Design

Fig. 2 shows a schematic of the Rx circuits, including a receiving resonant coil and a full-bridge rectifier. The input impedance, Z_{rx}, for the rectifier with matching network in the Rx is very important for designing the Tx and the resonant coils. R_L and C_L are a load resistance and a large capacitance of the rectifier to obtain appropriate dc voltage at the load. The matching network is designed using C_{r1}, C_{r2}, L_{r1}, and L_{r2}. The resonant capacitor, C_{rx}, and L_{r2}, can be merged with a single reactive component. Z'_{rx} is an input impedance of the rectifier. Z'_{rx} was calculated using fundamental components of current and voltage which were extracted using a large-signal simulation for the full-bridge rectifier. For the full-bridge rectifier, four Schottky diodes (Diodes, Inc.'s DFLS240 L) were used. The diode has a breakdown voltage of 40 V. For the three types of Rx's, an identical rectifier including the Rx matching network was used with L_{r1}, L_{r2}, C_{r1}, and C_{r2} of 1.5 μH, 0.75 μH, 370 pF, and 1500 pF, respectively.

Fig. 3 shows Z'_{rx} and Z_{rx} for two different R_L's of 10 and 20 Ω. R_L of 10 Ω was applied to obtain the received power levels of 40, 16, and 8 W for three types of the devices with output dc voltages of 20, 12, and 9 V, respectively. R_L of 20 Ω was also considered to design the overall transceiver, because the load resistance increases as the devices become more charged. The original input impedances of the rectifier (Z'_{rx}) are 6.6-j2.6 and 12.3-j5.9 Ω for R_L's of 10 and 20 Ω, respectively. After applying the matching network, the input impedances (Z_{rx}) become 25.7-j0.7 and 51.2-j6.8 Ω for R_L's of 10 and 20 Ω, respectively.

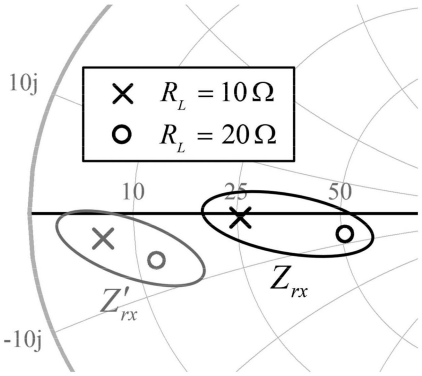

Fig. 3. Simulated Z'_{rx} and Z_{rx}.

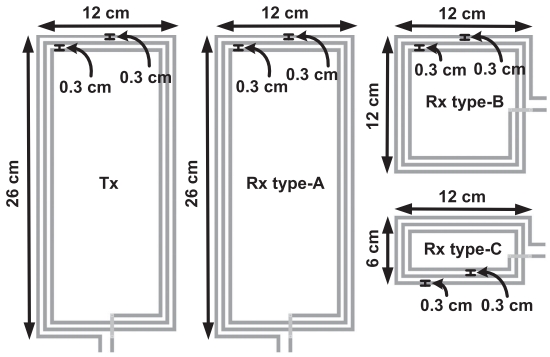

Fig. 4. Designed resonant coils for the Tx and three types of the Rx's.

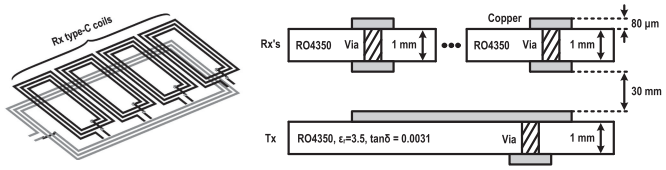

(a) (b)

Fig. 5. EM field simulation setup for the resonant coils. (a) 3-D view for Case 6. (b) PCB layers.

Fig. 4 shows the designed Tx coil and three different types of Rx coils. The size of the Tx and type-A Rx coils is 26×12 cm^2, and the sizes of the other two types of Rx coils are 12×12 and 6×12 cm^2. The width of the signal lines and line spacing are both 0.3 cm. The sizes of the Rx coils were determined by considering their applications, such as laptops, tablets, and cellular phones.

Fig. 5(a) shows a three dimensional (3-D) view of the electromagnetic field (EM) simulation setup using a single Tx coil and four type-C Rx coils for Case 6. The coils were implemented on a printed circuit board (PCB) based on Rogers Corp.'s RO4350 whose dielectric constant, loss tangent, thickness are 3.5, 0.0031, and 1.0 mm, respectively. The cross-sectional information for the simulation setup is depicted in Fig. 5(b). The top and bottom metal layers based on copper has a thickness of 80 μm.

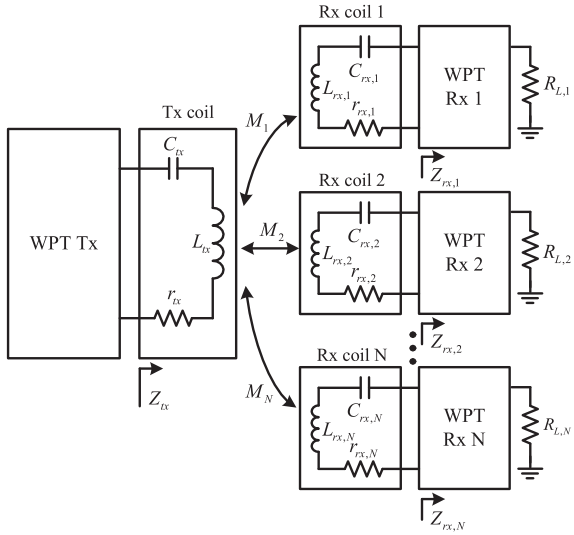

Fig. 6. WPT system with a Tx with multiple Rx's.

Keysight's momentum in the advanced design system (ADS) was used for the EM simulation.

C. Load Impedances of the Tx

Fig. 6 shows a WPT system with a Tx and multiple Rx's. For various configurations of multiple Rx's, the load impedances of the Tx (Z_{tx}) can differ. In the figure, C_{tx} and $C_{rx,N}$ are resonant capacitors for the coils of the Tx and *N*th Rx, respectively. L_{tx} and $L_{rx,N}$ are the self-inductances for the coils of the Tx and the *N*th Rx, respectively. M_N is the mutual inductance between the Tx coil and the *N*th Rx coil. The mutual inductances between the adjacent Rx coils were ignored based on the report by [17]. The load impedances of the Tx in perfect resonance are derived as follows.

$$Z_{tx} = r_{tx} + \sum_{i=1}^{N} \frac{\omega^2 M_i^2}{r_{rx,i} + Z_{rx,i}} \tag{1}$$

where r_{tx} and $r_{rx,i}$ are equivalent resistances to model the loss of the resonant coils for the Tx and *i*th Rx. As the Rx coil becomes smaller than the Tx coil, the mutual inductance, M, gets smaller, which decreases Z_{tx}. As the number of Rx's increases, Z_{tx} increases as well. If it is assumed that the equivalent resistances of the coils are very small, i.e. r_{tx}, $r_{rx,i} \approx 0$, and the mutual inductance of M_i remains large with enough Tx and Rx's coupling, and all the loads of the Rx are identical, the load impedances of the Tx can be simplified as follows.

$$Z_{tx} = \frac{Z_{0,coil}^2}{Z_{rx}} \tag{2}$$

$$Z_{0,coil} = \omega \sqrt{\sum\nolimits_{i=1}^{N} M_i^2}. \tag{3}$$

Equation (2) indicates that the resonant coils operate as an impedance transformer which works as a quarter-wave transmission line with a characteristic impedance of $Z_{0,coil}$ and an electrical length of 90°. The accurate values of Z_{tx}'s can be

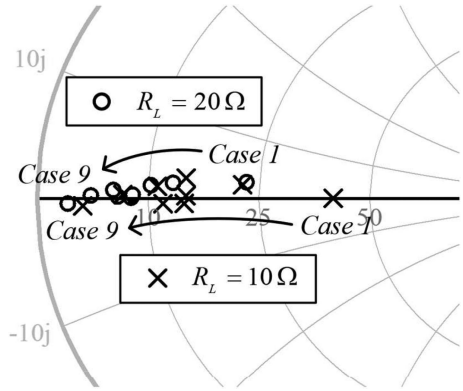

Fig. 7. Simulated Z_{tx}'s for various types of Rx configuration.

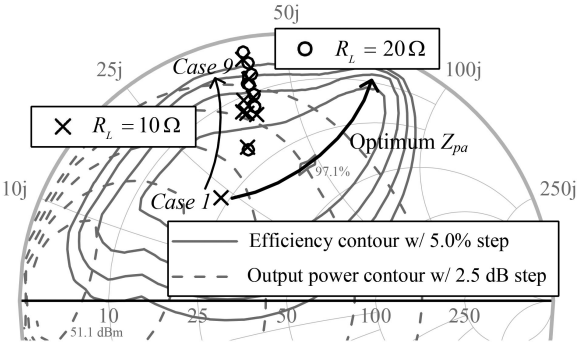

Fig. 9. Simulated Z_{pa}'s for the selected nine cases of the contours for constant efficiencies and constant output powers.

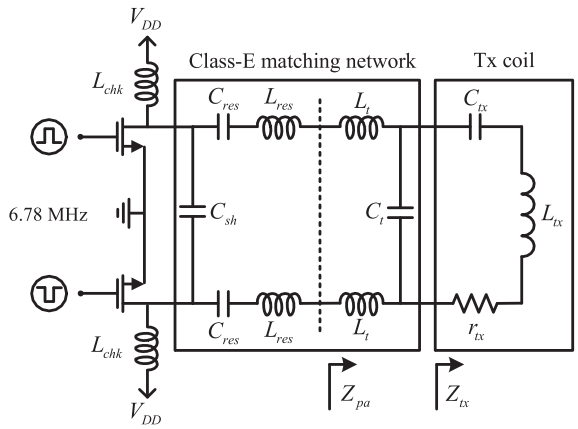

Fig. 8. Schematic of the differential Class–E PA with a Class–E load network and a Tx resonant coil.

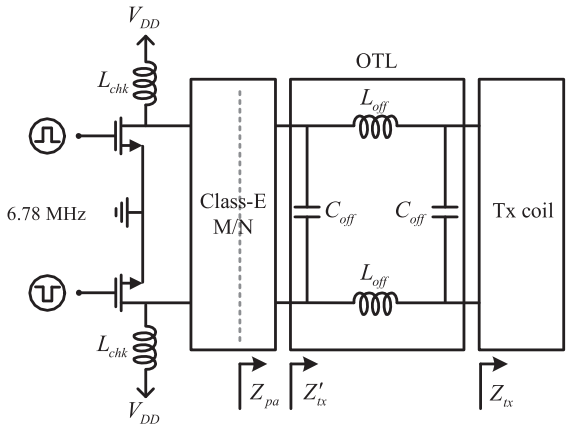

Fig. 10. Schematic of the differential Class–E PA with the OTL.

obtained using the EM simulation even including the effect of the mutual inductances between the adjacent Rx coils. For the cases with multiple Rx's, the cross-coupling between adjacent Rx coils was found to be negligible, so that it takes almost no effect on the output performances.

Fig. 7 shows the simulated Z_{tx}'s for the cases from 1 to 9 with Rx load resistances of 10 and 20 Ω. As shown, the widespread Z_{tx}'s for different cases, which are on the real axis of the Smith chart, must be matched for the PA of the Tx.

III. Reconfigurable Load Network Design for the Class–E PA

A. OTL of the Class–E PA

Fig. 8 shows a schematic of the differential Class–E PA with a Class–E load network and an equivalent circuit of the Tx resonant coil. L_{chk} is a large inductor for RF choke, and C_{sh} is a shunt capacitor required for Class–E operation. A series resonance network based on C_{res} and L_{res} follows. A low-pass L-section matching network using L_t and C_t transforms Z_{tx} to Z_{pa}.

Simulated load impedances, Z_{pa}'s, are presented in Fig. 9 on the contours for constant efficiencies with a step of 5% points and for constant output powers with a step of 2.5 dB. The simple L-section impedance matching network for the Class–E PA was designed to have high-efficiency and high output power especially for Case 1, which requires very high received power at the Rx of about 40 W for laptop applications. However, as shown, other impedances are dispersed and rotated away from the high-efficiency region.

Fig. 10 is a schematic of the differential Class–E PA including the OTL, which is designed to rotate Z_{tx} on the Smith chart. The OTL is designed using lumped components with a balanced π–type structure. With rotated load impedances of Z'_{tx}'s, the Z_{pa}'s can be rotated into the high-efficiency region, which is graphically presented in Fig. 9.

The values of the lumped components for the balanced π-type transmission line are given as follows.

$$L_{\text{off}} = \frac{Z_{0,off}\sin\theta}{\omega} \tag{4}$$

$$C_{\text{off}} = \frac{1}{2\omega Z_{0,off}}\sqrt{\frac{1-\cos\theta}{1+\cos\theta}} \tag{5}$$

where $Z_{0,off}$ and θ are a characteristic impedance and a phase angle of the line, respectively. The value of C_{off} must be half that of the shunt capacitor for the single-ended π–type transmission line based on lumped components. Then, the rotated load

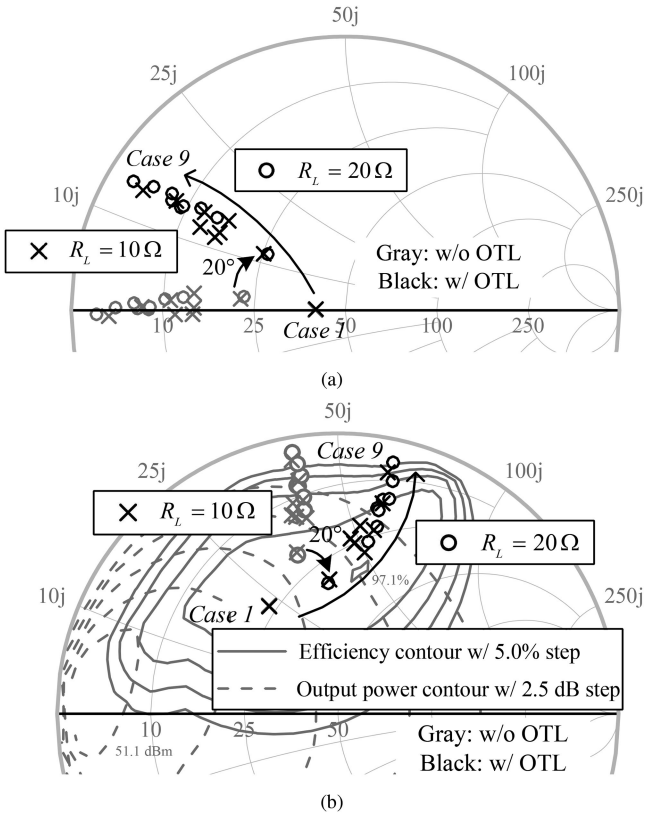

Fig. 11. Simulated impedances with and without OTL. (a) Z'_{tx}'s. (b) Z_{pa}'s.

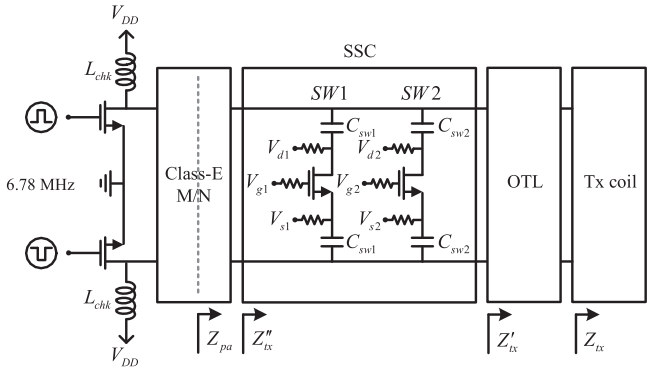

Fig. 12. Schematic of the Tx including the SSC.

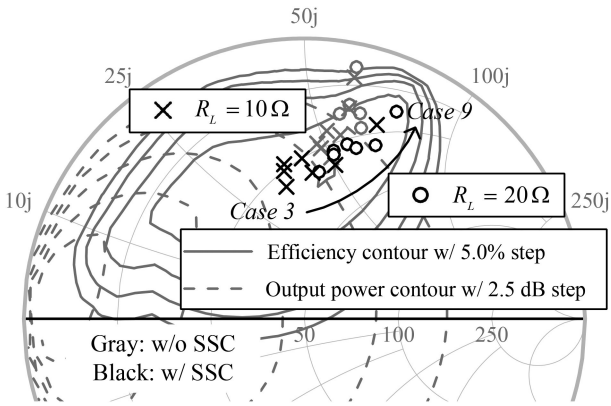

Fig. 13. Simulated Z_{pa}'s with and without SSC for the cases from 3 to 9.

impedance of Z'_{tx}'s can be obtained as follows.

$$Z'_{tx} = Z_{0,off}\frac{Z_{tx} + jZ_{0,off}\tan\theta}{Z_{0,off} + jZ_{tx}\tan\theta} \tag{6}$$

where the OTL is assumed as lossless.

The OTL having $Z_{0,off}$ of 40 Ω and θ of 20° was designed using (4) and (5) and applied between the load network of the Class-E PA and the Tx coil. Fig. 11 shows the simulated impedances with and without OTL. Fig. 11(a) shows Z'_{tx}'s that are rotated from Z_{tx}'s by 20° around the characteristic impedance of 40 Ω as a center. As a result, Z_{pa}'s are rotated in the high-efficiency region, as shown in Fig. 11(b). As shown, the OTL with appropriate characteristic impedance and phase can increase the efficiency of the Class-E PA for various cases.

For the load network of the Tx for WPT, some impedance matching networks, such as a single-ended π-type impedance matching network [11] and a double-sided LCC compensation network [22], were previously reported. However, these impedance matching networks were designed just for a single Rx. The proposed OTL operates as a transmission line with a constant characteristic impedance and a constant electrical length, which can transform the load impedances of the PA, to maintain high-efficiency for various configurations of the multiple Rx's.

B. SSC of the Class–E PA

In Fig. 11(b), Z_{pa}'s for cases 1 and 2 are matched well in the high power and efficiency region. However, as the case number increases to 9, Z_{pa}'s escape from the high power and efficiency region. To further improve the output power of the PA for the cases from 3 to 9, Z_{pa}'s for those cases must be shifted to the higher power and efficiency region.

Fig. 12 is a schematic of the Tx with the SSC that includes two parallel switching paths, consisting of one transistor and two capacitors of C_{sw1} and C_{sw2}. C_{sw1} is smaller than C_{sw2}. Switch control voltages of V_g, V_s, and V_d are supplied through 10 kΩ resistors. The switch can be turned on by applying a high voltage of 20 V to V_g and a low voltage of 0 V to V_d and V_s. For this condition, a capacitance of C_{sw}/2 is added in parallel to the network. If the switch is turned OFFby applying high voltage to V_d and V_s and low voltage to V_g, no additional capacitance is added to the network. The load admittance of Y'_{tx} which is $1/Z'_{tx}$ can be changed to be Y''_{tx} according to the states of the switches as follows.

$$Y''_{tx} = \begin{cases} Y'_{tx}, & \text{both SWs OFF} \\ Y'_{tx} + j\omega\dfrac{C_{sw1}}{2}, & \text{SW1: on and SW2: OFF} \\ Y'_{tx} + j\omega\dfrac{C_{sw2}}{2}, & \text{SW1: off and SW2: ON.} \end{cases} \tag{7}$$

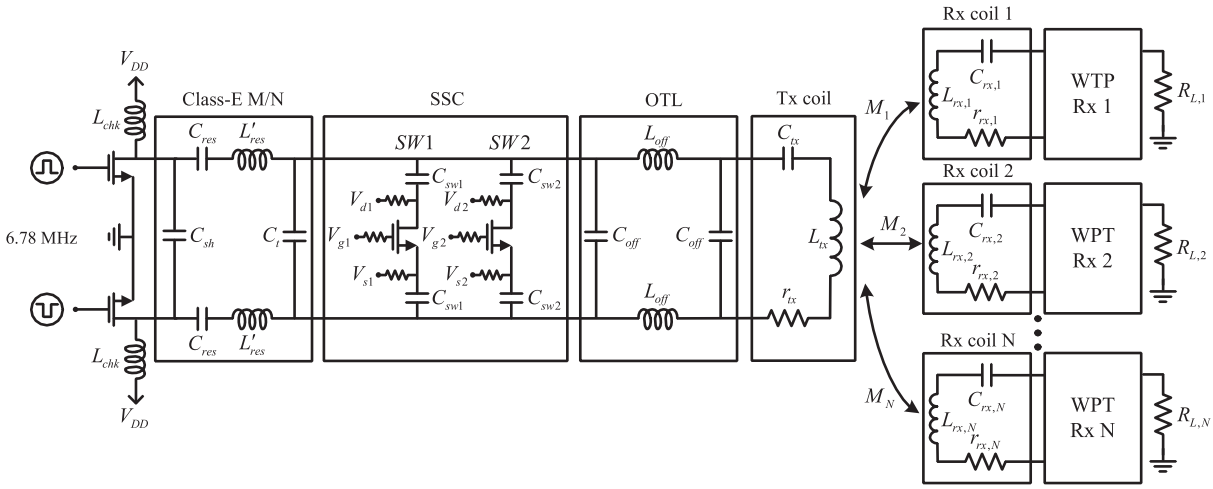

Fig. 14. Schematic of the proposed WPT Tx with multiple Rx's.

Then, Z_{pa}'s are changed according to the Z''_{tx} which is $1/Y''_{tx}$ as follows.

$$Z_{pa} = \frac{1}{Y''_{tx} + j\omega C_t} + j\omega 2L_t \tag{8}$$

where L_t and C_t are a series inductor and a shunt capacitor, respectively, for impedance matching.

An adaptive matching network based on the capacitor matrix switching [22] requires many capacitors and switches. As the number of switches increases, the control circuit and algorithm become more complex and the time for adaptive control can be significantly increased. However, the proposed SSC has just two essential switches which were realized using transistors in small surface-mountable packages instead of relay-based switches used in [22].

Fig. 13 shows simulated Z_{pa}'s with and without SSC for the cases from 3 to 9. The switch, SW1, is turned ON for the cases from 3 to 7, whereas SW2 is turned ON for cases 8 and 9. With SSC, Z_{pa}'s are shifted to the high power and efficiency region, which increases the output power and efficiency of the PA for each case.

IV. Implementation and Experimental Results

Fig. 14 is a schematic of the proposed WPT Tx with multiple Rx's. Two switching transistors (Fairchild's fdmc86248) are used for the differential Class-E PA. Differential input signal with a frequency of 6.78 MHz is applied to the gates of the transistors. A V_{DD} of 20 V is applied through L_{chk} to the drains of the transistors. Two series inductors of L_{res} and L_t are merged to a single inductor of L'_{res} at the Class–E matching network. The OTL is designed to improve efficiency of the Class–E PA for various cases. In addition, the SSC is added to further improve the output power and efficiency of the PA for the cases from 3 to 9. For the SSC, switching transistors (Fairchild's fdmc86248) are employed to switch the shunt capacitors of C_{sw1} and C_{sw2}. The proposed WPT Tx for multiple device charging was designed and implemented. The component values and design parameters for the proposed WPT Tx are listed in Table II. Quality factors of the coils are computed as 194, 183, and 147 for Rx type A (or Tx), B, and C, respectively.

TABLE II
Component Values and Design Parameters for the Proposed WPT Tx

Component	Value	Component	Value
L'_{res}	1.0 μH	C_{sh}	100 pF
L_{off}	0.18 μH	C_t	500 pF
L_{tx}	3.74 μH	C_{res}	1100 pF
$L_{rx,1}$	3.74 μH	C_{sw1}	820 pF
$L_{rx,2}$	1.96 μH	C_{sw2}	1100 pF
$L_{rx,3}$	1.14 μH	C_{off}	100 pF
r_{tx}	0.823 Ω	C_{tx}	147 pF
$r_{rx,1}$	0.823 Ω	$C_{rx,1}$	147 pF
$r_{rx,2}$	0.457 Ω	$C_{rx,2}$	281 pF
$r_{rx,3}$	0.331 Ω	$C_{rx,3}$	484 pF

Fig. 15(a) and (b) are photographs of the implemented Tx and the full–bridge rectifier for the WPT system. The Tx includes the proposed OTL and SSC and has a size of 13.0×8.5 cm^2. Both the Tx and rectifier were implemented on a PCB based on FR4. The full-bridge rectifier including the Rx matching network has a size of 3.5×2.5 cm^2. Fig. 16 shows examples of the measurement setups for various cases of multiple charging: (a) Case 1, (b) Case 2, and (c) Case 6. A supply voltage of 20 V is applied to the Tx using a dc power supply. Electrical loads (Maynuo's M9712 and Keithley's 2380) provide the load resistances of the Rx's and the waveforms were probed using an oscilloscope (Keysight's DSOX1120 G). The received output power was calculated using the measured dc voltage and the load resistance. Considering the thickness of the housing of each device, the distances between Tx coil and Rx coils were set as 50, 40, and 30 mm for Rx types A, B, and C, respectively.

Fig. 17 shows the measured voltage waveforms for the implemented WPT system. $V_{G,P}$ and $V_{G,N}$ are the gate voltages for the positive and negative transistor cells. $V_{D,P}$ and $V_{D,N}$ are the drain voltages for the positive and negative transistor cells for

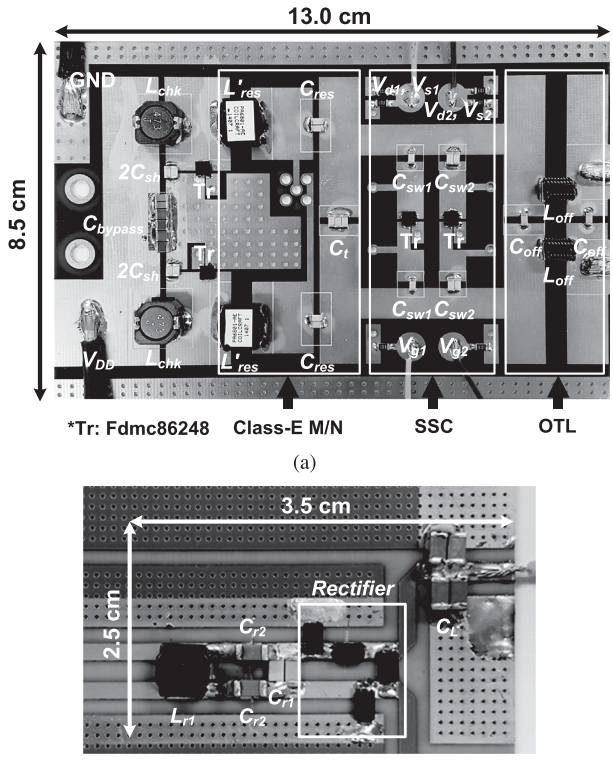

Fig. 15. Photographs of the implemented Tx (in(a)) and full–bridge rectifier including the Rx matching network (in(b)) for the proposed WPT system.

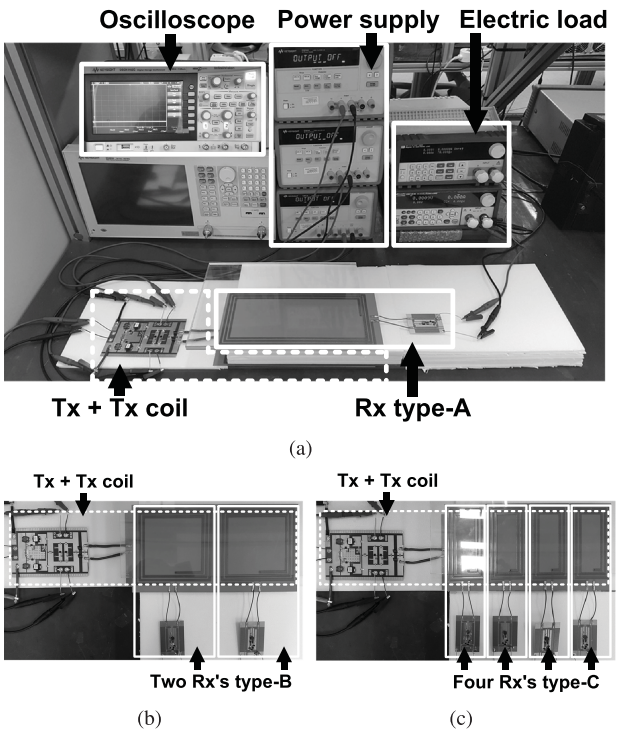

Fig. 16. Examples for the measurement setups for the proposed WPT system. (a) Case 1. (b) Case 2. and (c) Case 6.

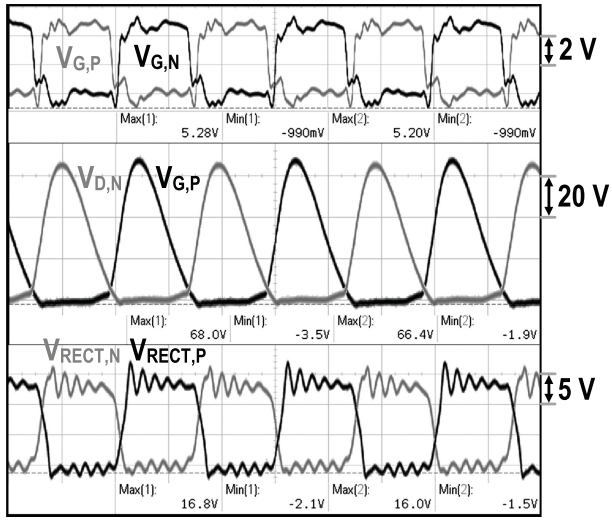

Fig. 17. Measured voltage waveforms for the proposed WPT system.

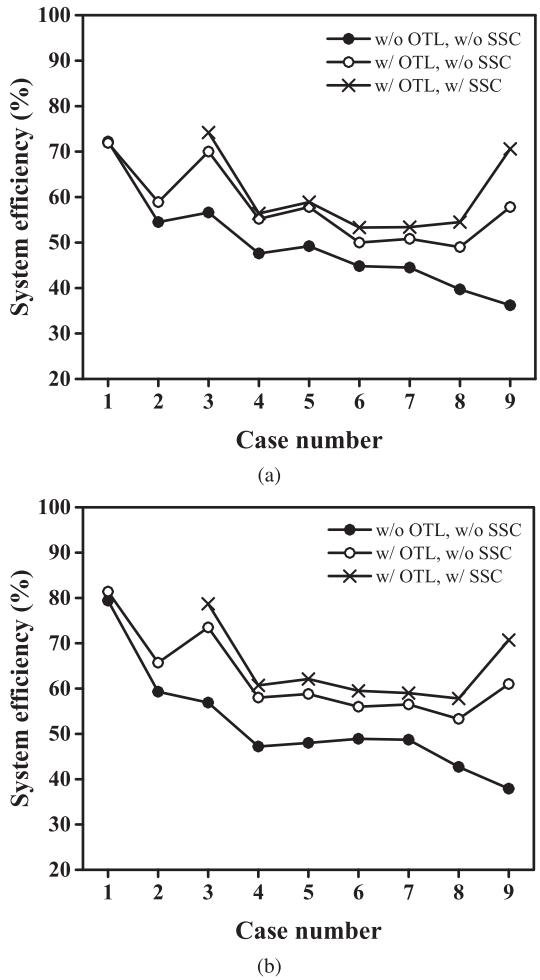

Fig. 18. Measured system efficiencies for the cases from 1 to 9. (a) R_L of 10 Ω. (b) R_L of 20 Ω.

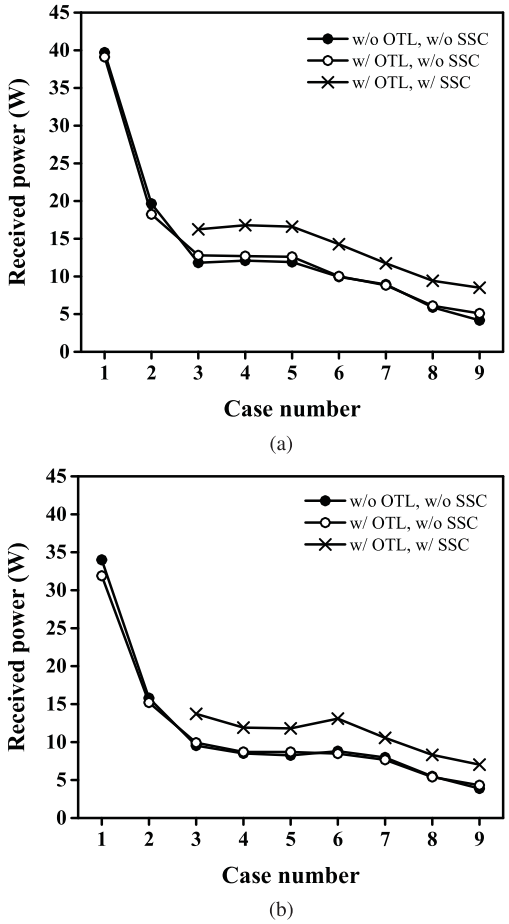

Fig. 19. Measured received dc powers for the cases from 1 to 9. (a) R_L of 10 Ω. (b) R_L of 20 Ω.

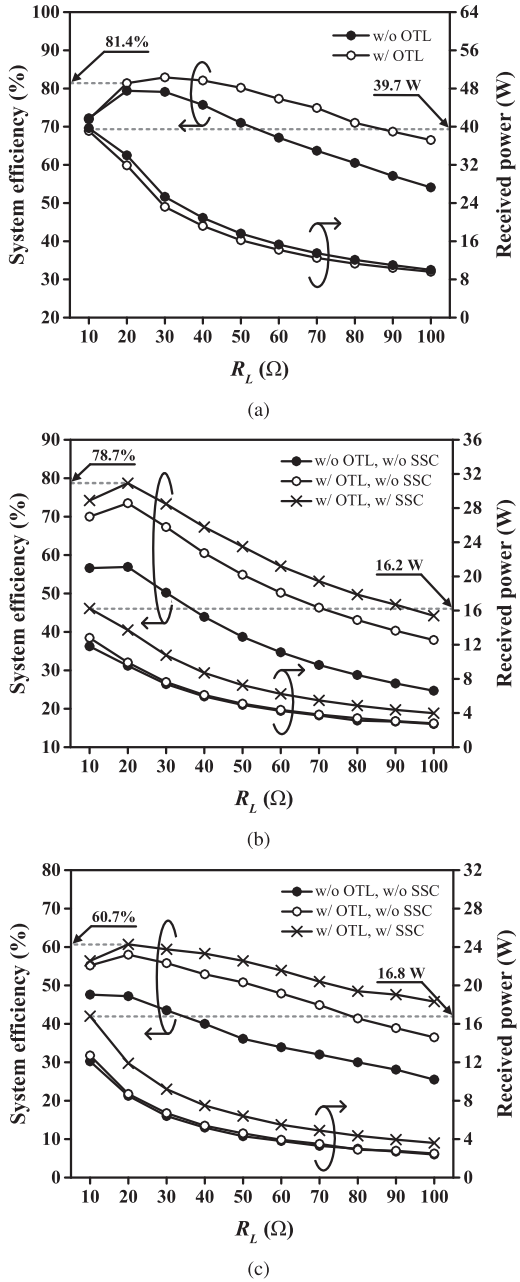

Fig. 20. Measured system efficiencies and received dc powers for various R_L's. (a) Case 1. (b) Case 3. (c) Case 4.

the differential Class-E PA. Peak voltage of about 68 V, which is 3.4 times larger than the supply voltage of 20 V, was measured. $V_{RECT,P}$ and $V_{RECT,N}$ are the measured voltages at the input ports of the full-bridge rectifier. Fig. 18 shows the measured system efficiencies of the proposed Tx and Rx's, including Class-E PA, Tx and Rx coils, Rx rectifier, for the cases from 1 to 9 with the Rx load resistance (R_L) of 10 Ω [for (a)] and 20 Ω [for (b)]. Since the system includes the single-stage differential Class-E PA, OTL, SSC, Tx/Rx coils, and the full-bridge rectifier, the system efficiency was calculated using the power sum from all the dc outputs of the rectifiers divided by the dc power supplied to the Class-E PA.

Compared to the efficiency without the proposed OTL and SSC networks, the measured efficiencies for the cases from 2 to 9 were clearly improved by using the proposed OTL. In addition, the measured efficiencies for the cases from 3 to 9 can be further improved by using the proposed SSC. For Case 1, with an R_L of 20 Ω, a high-efficiency of 81.4% was achieved. The received power of each Rx for the cases with multiple Rx's (case 2, 4, 5, 6, 7, and 8) becomes a little lower than the received power for the cases with a single Rx (case 1, 3, and 9). Since the RF-dc conversion efficiency of the full-bridge rectifier decreases as the RF input power decreases, the efficiencies for the cases with multiple Rx's become a little lower than those for the cases with a single Rx.

Fig. 19 shows the measured received dc powers for the cases from 1 to 9 with the Rx load resistance (R_L) of 10 Ω [for (a)] and 20 Ω [for (b)]. Compared to the received dc powers without the SSC, the received dc powers are clearly increased for the cases from 3 to 9. For the cases with a single Rx, such as 1, 3, and 9, the received dc powers are 39.7, 16.3, and 8.5 W, which can sufficiently charge laptops, tablets, and mobile phones, respectively. In other multiple Rx cases, sufficient dc power was received from the multiple Rx's. The measured performances are summarized for all the cases in Table III.

TABLE III
PERFORMANCE SUMMARY OF THE PROPOSED WIRELESS POWER TRANSFER SYSTEM FOR THE CASES OF VARIOUS RECEIVERS

Charging case	Case1	Case2	*Case3	*Case4	*Case5	*Case6	*Case7	*Case8	*Case9
Rx configuration	One type–A	Two type–B	One type–B	One type–B Two type–C	One type–B One type–C	Four type–C	Three type–C	Two type–C	One type–C
R_L = 10 Ω	39.7 W 71.9%	18.3 W 58.9%	16.2 W 74.2%	16.8 W 56.4%	16.6 W 58.9%	14.3 W 53.3%	11.7 W 53.4%	9.4 W 54.5%	8.5 W 70.6%
R_L = 20 Ω	31.9 W 81.4%	15.2 W 65.7%	13.7 W 78.7%	11.9 W 60.7%	11.8 W 62.1%	13.1 W 59.5%	10.6 W 59.0%	8.3 W 57.8%	7.0 W 70.7%

*: Susceptance is tuned using the SSC.

TABLE IV
PERFORMANCE COMPARISON OF THIS RESEARCH AND PREVIOUS STUDIES

Ref.	Tx coil size (cm^2)	Rx coil size (cm^2)	Number of Rx's	Type of the PA	Supply voltage (V)	Peak received power (W)	Peak system efficiency (%)	Rx configuration	Features
[10]	10×10	10×10	1	Class–E	18	20.0	84.0	Single	Parameter optimization for load variation
[11]	10×10	10×10	1	†CM Class–E ††VM Class–E	25	*27.0	*81.0	Single	‡ITN for wide load variation
[12]	21×14	6×4.4	1	Class–D	N/A	5.0	*54.0	Single	Closed–loop control for ‡‡MET
[13]	20×10	10×6	3	CM Class–E	30	20.0	71.7	Homogeneous multiple	Closed–loop control for ‡‡MET
[14]	314	32	6	Class–E	35	*27.8	*74.7	Homogeneous multiple	Battery voltage equalization process
[22]	1256	1256	1	Class–E	N/A	1.0	88.0	Single	Adaptive matching for distance variation
In this work	26×12	26×12 12×12 6×12	1, 2, 3, 4	Differential Class–E	20	39.7 16.3/1 Rx 8.5/1 Rx	81.4 78.7 70.7	Single, homogeneous multiple, and heterogeneous multiple	OTL and SCC for various Rx configurations

*Graphically estimated, N/A: not available,
†Current mode,
††Voltage mode,
‡Impedance transformation network,
‡‡Maximum efficiency tracking

Fig. 20 shows the measured system efficiencies and received dc powers for various R_L's. The measured efficiencies were significantly improved using the proposed OTL for the R_L's of from 10 to 100 Ω for the all charging cases from 1 to 9. From Case 3 to 9, the efficiencies were further improved using not only the OTL but also the SSC. The received dc powers were maintained for Case 1 and 2 only using the OTL but were increased for Case 3–9 using both the OTL and SSC.

Fig. 21 shows the estimated loss of each circuit block for the all cases with the Rx load resistance of 10 Ω. For the cases of 1 and 2, the losses were estimated for the configurations without and with OTL. For the cases of from 3 to 9, the losses were estimated for the configurations without and with both OTL and SSC. For the case 2, since the loss of the switch is drastically reduced for the configuration with OTL, the system efficiency is accordingly increased. For the cases of from 3 to 9, the system efficiencies are increased due to the decreased loss of the switch and the increased output power by turning SSC on.

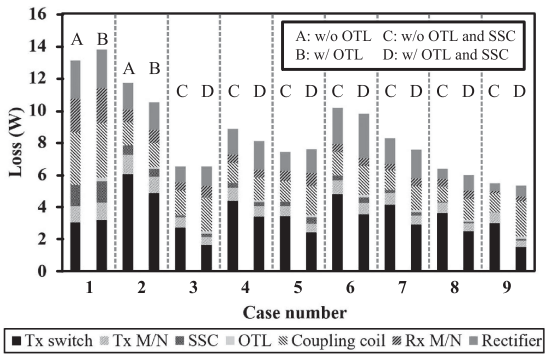

Fig. 21. Loss estimation for the circuit blocks.

The performances and configurations of the designed WPT system are summarized and compared to the previously reported 6.78 MHz WPT systems in Table IV. Compared to the previous

work with multiple Rx's, the proposed WPT system exhibited higher efficiency for various Rx configurations.

V. Conclusion

In this article, a 6.78 MHz WPT Tx based on a differential Class-E PA with the proposed OTL and SSC was presented for transmitting power to multiple Rx's based on various different types of Rx. The differential Class-E PA was adopted to have higher output power than the single-ended PA's using the same supply voltage. To improve the power transfer efficiency for the selected cases with various Rx configurations, the OTL was proposed to shift the load impedances of the PA to the high-efficiency region. In addition, to further increase the received dc power for some cases, the SSC was proposed to shift the load impedances of the PA to the high power and efficiency region.

To validate the proposed methods, a differential Class-E PA including the OTL and SSC, Tx coil, Rx coils for various Rx types, and bridge-diode rectifiers were implemented. The system efficiencies and received dc powers of the implemented WPT systems for the various multiple charging configurations were measured in three conditions: without OTL and SSC, with OTL but without SSC, and with both OTL and SSC. With the proposed OTL and SSC, the system efficiencies and received dc power levels were clearly improved for the aimed cases. For the three different types of single Rx, received dc powers of 39.7, 16.3, and 8.5 W, which are sufficient to charge laptops, tablets, and mobile phones, were achieved. A peak system efficiency of 81.4% was achieved for the Rx type-A. Compared to the previous WPT systems for multiple Rx's, the proposed system has advantages in charging various types of single and multiple devices while maintaining very high–efficiency and sufficient received power for each case.

References

[1] A. Kurs, A. Karalis, R. Moffatt, J. D. Joannopoulos, P. Fisher, and M. Soljacic, "Wireless power transfer via strongly coupled magnetic resonances," *Science*, vol. 317, no. 5834, pp. 83–86, Jul. 2007.

[2] Y.-J. Kim, D. Ha, W. J. Chappell, and P. P. Irazoqui, "Selective wireless power transfer for smart power distribution in a miniature-sized multiple–receiver system," *IEEE Trans. Ind. Electron.*, vol. 63, no. 3, pp. 1853–1862, Mar. 2016.

[3] H. Hwang, J. Moon, B. Lee, C. H. Jeong, and S. W. Kim, "An analysis of magnetic resonance coupling effects on wireless power transfer by coil inductance and placement," *IEEE Trans. Consum. Electron.*, vol. 60, no. 2, pp. 203–209, May 2014.

[4] H. Yin, M. Fu, M. Liu, J. Song, and C. Ma, "Autonomous power control in a reconfigurable 6.78–MHz multiple–receiver wireless charging system," *IEEE Trans. Ind. Electron.*, vol. 65, no. 8, pp. 6177–6187, Aug. 2018.

[5] E. S. G. Rodrguez, A. K. RamRakhyani, D. Schurig, and G. Lazzi, "Compact low–frequency metamaterial design for wireless power transfer efficiency enhancement," *IEEE Trans. Microw. Theory Techn.*, vol. 64, no. 5, pp. 1644–1654, May 2016.

[6] M. Liu, C. Zhao, J. Song, and C. Ma, "Battery charging profile–based parameter design of a 6.78-MHz class E^2 wireless charging system," *IEEE Trans. Ind. Electron.*, vol. 64, no. 8, pp. 6169–6178, Aug. 2017.

[7] Z. Liu, Z. Zhong, and Y.-X. Guo, "*In vivo* high–efficiency wireless power transfer with multisine excitation," *IEEE Trans. Microw. Theory Techn.*, vol. 65, no. 9, pp. 3530–3540, Sep. 2017.

[8] S. Li, Z. Liu, H. Zhao, L. Zhu, C. Shuai, and Z. Chen, "Wireless power transfer by electric field resonance and its application in dynamic charging," *IEEE Trans. Ind. Electron.*, vol. 63, no. 10, pp. 6602–6612, Oct. 2016.

[9] K. Xie, A. Huang, L. Chen, S. Guo, and H. Zhang, "Half-cycle resonance tracking for inductively coupled wireless power transmission system," *IEEE Trans. Power Electron.*, vol. 33, no. 3, pp. 2668–2679, Mar. 2018.

[10] M. Liu, M. Fu, and C. Ma, "Parameter design for a 6.78 MHz wireless power transfer system based on analytical derivation of Class E current driven rectifier," *IEEE Trans. Power Electron.*, vol. 31, no. 6, pp. 4280–4291, Jun. 2016.

[11] S. Liu, M. Liu, S. Yang, C. Ma, and X. Zhu, "A novel design methodology for high–efficiency current-mode and voltage-mode Class–E power amplifiers in wireless power transfer systems," *IEEE Trans. Power Electron.*, vol. 31, no. 9, pp. 6524–6533, Sep. 2016.

[12] T. D. Yeo, D. Kwon, S. T. Khang, and J. W. Yu, "Design of maximum efficiency tracking control scheme for closed-loop wireless power charging system employing series resonant tank," *IEEE Trans. Power Electron.*, vol. 32, no. 1, pp. 471–478, Jan. 2017.

[13] M. Fu, H. Yin, and C. Ma, "Megahertz multiple-receiver wireless power transfer systems with power flow management and maximum efficiency point tracking," *IEEE Trans. Microw. Theory Techn.*, vol. 65, no. 11, pp. 4285–4293, Nov. 2017.

[14] M. Liu, M. Fu, Y. Wang, and C. Ma, "Battery cell equalization via megahertz multiple-receiver wireless power transfer," *IEEE Trans. Power Electron.*, vol. 33, no. 5, pp. 4135–4144, May 2018.

[15] M. Fu, Z. Tang, M. Liu, C. Ma, and X. Zhu, "Full-bridge rectifier input reactance compensation in megahertz wireless power transfer systems," presented at the IEEE PELS Workshop Emerg. Technol., Wireless Power, Daejeon, Korea, Jun. 2015.

[16] S. Liu, M. Liu, S. Han, X. Zhu, and C. Ma, "Tunable class E^2 DCDC converter with high–efficiency and stable output power for 6.78 MHz wireless power transfer," *IEEE Trans. Power Electron.*, vol. 33, no. 8, pp. 6877–6886, Aug. 2018.

[17] M. Fu, T. Zhang, C. Ma, and X. Zhu, "Efficiency and optimal loads analysis for multiple-receiver wireless power transfer systems," *IEEE Trans. Microw. Theory Techn.*, vol. 63, no. 3, pp. 801–812, Mar. 2015.

[18] S. Aldhaher, P. C.-K. Luk, and J. F. Whidborne, "Electronic tuning of misaligned coils in wireless power transfer systems," *IEEE Trans. Power Electron.*, vol. 29, no. 11, pp. 5975–5982, Nov. 2014.

[19] X. Liu, G. Wang, and W. Ding, "Efficient circuit modelling of wireless power transfer to multiple devices," *IET Power Electron.*, vol. 7, no. 12, pp. 3017–3022, 2014.

[20] J. Kim, D. Kim, and Y. Park, "Free-positioning wireless power transfer to multiple devices using a planar transmitting coil and switchable impedance matching networks," *IEEE Trans. Microw. Theory Techn.*, vol. 64, no. 11, pp. 3714–3722, Nov. 2016.

[21] K. E. Koh, T. C. Beh, T. Imura, and Y. Hori, "Impedance matching and power division using impedance inverter for wireless power transfer via magnetic resonant coupling," *IEEE Trans. Ind. Appl.*, vol. 50, no. 3, pp. 2061–2070, May/Jun. 2014.

[22] Y. Lim, H. Tang, S. Lim, and J. Park, "An adaptive impedance-matching network based on a novel capacitor matrix for wireless power transfer," *IEEE Trans. Power Electron.*, vol. 29, no. 8, pp. 4403–4413, Aug. 2014.

[23] S. Li, W. Li, J. Deng, T. D. Nguyen, and C. C. Mi, "A double-sided LCC compensation network and its tuning method for wireless power transfer," *IEEE Trans. Veh. Technol.*, vol. 64, no. 6, pp. 2261–2273, Jun. 2015.

[24] B.-C. Park and J.-H. Lee, "Adaptive impedance matching of wireless power transmission using multi–loop feed with single operating frequency," *IEEE Trans. Antennas Propag.*, vol. 62, no. 5, pp. 2851–2856, May 2014.

Hansik Oh was born in Seoul, South Korea, in 1991. He received the B.S. degree from Sungkyunkwan University, Suwon, South Korea, in 2016. He is currently working toward the Ph.D. degree with the Department of Electrical and Computer Engineering, Sungkyunkwan University, Suwon, Korea.

His research interests include the design of RF/mm-wave power amplifiers, RF/analog integrated circuit, efficiency enhancement techniques, linearization techniques, broadband techniques, and wireless power transfer system.

Wooseok Lee (S'19) was born in Daejeon, Korea, in 1989. He received the B.S. degree in electronic engineering from Chungnam University, Daejeon, South Korea, in 2014. He is currently working toward the Ph.D. degree with the department of information and communication engineering, Sungkyunkwan University, Suwon, Korea.

His research interests include the design of RF/mm-wave power amplifiers, efficiency enhancement techniques, linearization techniques, broadband techniques, and mm-wave integration circuits and systems.

Hyungmo Koo was born in Seoul, South Korea, in 1992. He received the B.S. degree from Sungkyunkwan University, Suwon, South Korea, in 2016. He is currently working toward the Ph.D. degree with the Department of Information and Communication Engineering, Sungkyunkwan University, Suwon, Korea.

His current research interests include the design of RF power amplifiers, efficiency enhancement techniques, transceiver arrays, microwave power transmission, and passive circuits optimizations.

Jongseok Bae (S'19) was born in Suwon, Korea, in 1987. He received the B.S. degrees in electronic engineering from Chungnam University, Daejeon, South Korea, in 2014. He is currently working toward the Ph.D. degree with the Department of Electrical and Computer Engineering, Sungkyunkwan University, Suwon, Korea.

His research interests include the design of RF power amplifiers, efficiency enhancement techniques, wireless power transfer, and RF energy harvesting.

Keum Cheol Hwang (SM'13) received the B.S. degree in electronics engineering from Pusan National University, Busan, Korea, in 2001, and M.S. and Ph.D. degrees in electrical and electronic engineering from the Korea Advanced Institute of Science and Technology, Daejeon, South Korea, in 2003 and 2006, respectively.

From 2006 to 2008, he was a Senior Research Engineer with Samsung Thales, Yongin, South Korea, where he was involved with the development of various antennas including multiband fractal antennas for communication systems and Cassegrain reflector antenna and slotted waveguide arrays for tracking radars. He was an Associate Professor with the Division of Electronics and Electrical Engineering, Dongguk University, Seoul, Korea, from 2008 to 2014. In 2015, he joined the Department of Electrical and Computer Engineering, Sungkyunkwan University, Suwon, South Korea, where he is now an Associate Professor. His research interests include advanced electromagnetic scattering and radiation theory and applications, design of multi-band/broadband antennas and radar antennas, and optimization algorithms for electromagnetic applications.

Prof. Hwang is a Life Member of KIEES and a member of IEICE.

Kang-Yoon Lee (M'05–SM'10) received the B.S., M.S., and Ph.D. degrees from the School of Electrical Engineering, Seoul National University, Seoul, Korea, in 1996, 1998, and 2003, respectively.

From 2003 to 2005, he was with GCT Semiconductor Inc., San Jose, CA, USA, where he was a Manager with the Analog Division and worked on the design of CMOS frequency synthesizer for CDMA/PCS/PDC and single-chip CMOS RF chip sets for W-CDMA, WLAN, and PHS. From 2005 to 2011, he was with the Department of Electronics Engineering, Konkuk University, Seoul, South Korea, as an Associate Professor. Since 2012, he has been with the Department of Electrical and Computer Engineering, Sungkyunkwan University, Suwon, South Korea, where he is currently an Associate Professor. His research interests include implementation of power integrated circuits, CMOS RF transceiver, analog integrated circuits, and analog/digital mixed-mode VLSI system design.

Youngoo Yang (S'99–M'02–SM'15) was born in Hamyang, South Korea, in 1969. He received the Ph.D. degree in electrical and electronic engineering from the Pohang University of Science and Technology (Postech), Pohang, South Korea, in 2002.

From 2002 to 2005, he was with Skyworks Solutions Inc., Newbury Park, CA, USA, where he designed power amplifiers for various cellular handsets. Since March 2005, he has been with the Department of Electrical and Computer Engineering, Sungkyunkwan University, Suwon, Korea, where he is currently a Professor. His research interests include RF/mm–wave power amplifiers, RF transmitters, and dc–dc converters.